Molecular Therapy
Original Article

Evidence in primates supporting the use of chemogenetics for the treatment of human refractory neuropsychiatric disorders

Patrick H. Roseboom,[1,5] Sascha A.L. Mueller,[1,5] Jonathan A. Oler,[1] Andrew S. Fox,[2] Marissa K. Riedel,[1] Victoria R. Elam,[1] Miles E. Olsen,[1] Juan L. Gomez,[3] Matthew A. Boehm,[3] Alexandra H. DiFilippo,[4] Bradley T. Christian,[1,4] Michael Michaelides,[3] and Ned H. Kalin[1]

[1]Department of Psychiatry and the HealthEmotions Research Institute, University of Wisconsin School of Medicine and Public Health, Madison, WI 53719, USA; [2]Department of Psychology and the California National Primate Research Center, University of California-Davis, Davis, CA 95616, USA; [3]Biobehavioral Imaging and Molecular Neuropsychopharmacology Unit, National Institute on Drug Abuse Intramural Research Program, National Institutes of Health, Baltimore, MD 21224, USA; [4]Department of Medical Physics, University of Wisconsin School of Medicine and Public Health, Madison, WI 53705, USA

Non-human primate (NHP) models are essential for developing and translating new treatments that target neural circuit dysfunction underlying human psychopathology. As a proof-of-concept for treating neuropsychiatric disorders, we used a NHP model of pathological anxiety to investigate the feasibility of decreasing anxiety by chemogenetically (DREADDs [designer receptors exclusively activated by designer drugs]) reducing amygdala neuronal activity. Intraoperative MRI surgery was used to infect dorsal amygdala neurons with AAV5-hSyn-HA-hM4Di in young rhesus monkeys. *In vivo* microPET studies with [^{11}C]-deschloroclozapine and postmortem autoradiography with [^{3}H]-clozapine demonstrated selective hM4Di binding in the amygdala, and neuronal expression of hM4Di was confirmed with immunohistochemistry. Additionally, because of its high affinity for DREADDs, and its approved use in humans, we developed an individualized, low-dose clozapine administration strategy to induce DREADD-mediated amygdala inhibition. Compared to controls, clozapine selectively decreased anxiety-related freezing behavior in the human intruder paradigm in hM4Di-expressing monkeys, while coo vocalizations and locomotion were unaffected. These results are an important step in establishing chemogenetic strategies for patients with refractory neuropsychiatric disorders in which amygdala alterations are central to disease pathophysiology.

INTRODUCTION

Anxiety disorders are among the most prevalent psychiatric illnesses and, despite currently available treatments, remain a major public health concern.[1,2] As such, there is a critical need to develop novel and improved treatment strategies. Anxiety disorders frequently begin in childhood, and by using our young rhesus monkey model of pathological anxiety, we identified the neural circuit and molecular substrates relevant to understanding the childhood risk to develop anxiety disorders.[3–12] The evolutionary relatedness of non-human primates (NHPs) to humans enables an opportunity to perform proof-of-concept studies in this highly translational model[13–18] that is directly relevant to human psychiatric illnesses. Our NHP work, modeling pathological anxiety or anxious temperament (AT), has demonstrated involvement of the dorsal amygdala, including regions such as the central nucleus (Ce) and dorsal aspects of the basolateral nuclei.[3,5,7,19] Here, to further investigate mechanisms underlying primate anxiety, and as a model for potential human use, we use DREADDs (designer receptors exclusively activated by designer drugs) to reversibly manipulate neurons within the dorsal amygdala.[20–22] Demonstrating the ability to manipulate neural circuits using chemogenetic methods to reduce NHP anxiety is an important step toward developing novel treatments for refractory psychiatric illnesses, including severe human anxiety disorders.

DREADDs provide the ability to regulate the function of select brain circuits, which could lead to the development of specific neural circuit interventions, enabling personalized treatment strategies.[22] The most common DREADD method uses viral vector mediated gene delivery to induce cellular expression of mutated muscarinic receptors (hM3Dq, activating; hM4Di, inhibiting) that are not responsive to endogenous acetylcholine.[20] The ability to modulate DREADD-expressing cells requires the administration of a DREADD-activating selective ligand. DREADDs, and other chemogenetic methods, are particularly suitable for potential human interventions as the modulation of specific neural circuits can be accomplished via the oral or parenteral administration of DREADD-activating drugs. Establishing

Received 17 January 2021; accepted 16 April 2021;
https://doi.org/10.1016/j.ymthe.2021.04.021.

[5]These authors contributed equally

Correspondence: Patrick H. Roseboom, Department of Psychiatry and the HealthEmotions Research Institute, University of Wisconsin School of Medicine and Public Health, Madison, WI 53719, USA.
E-mail: roseboom@wisc.edu

Please cite this article in press as: Roseboom et al., Evidence in primates supporting the use of chemogenetics for the treatment of human refractory neuropsychiatric disorders, Molecular Therapy (2021), https://doi.org/10.1016/j.ymthe.2021.04.021

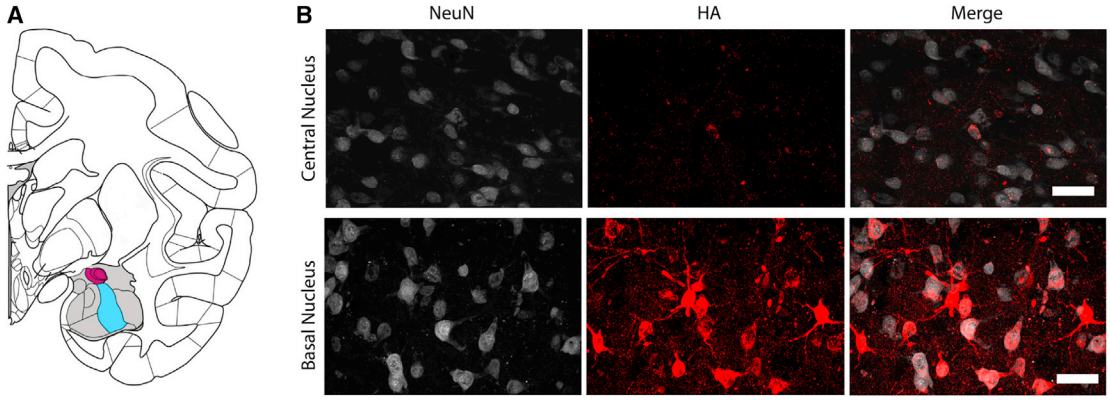

Figure 1. Representative images of hM4Di-HA expression in the rhesus amygdala

(A) The rhesus amygdala is composed of several nuclei, of which the central nucleus (medial and lateral divisions in purple) and basal nucleus (magnocellular and intermediate divisions in blue) were stereologically analyzed in subject P1. (B) Co-labeling of NeuN (left panels; greyscale) and HA (middle panels; red) in subject P1 revealed that neuronal expression of hM4Di-HA varied between subregions of the amygdala, with little coexpression observed in the central nucleus (top panels) compared to the magnocellular and intermediate portions of the basal nucleus (bottom panels). Images are maximum intensity projections integrated across the z stack. Scale bar (white) is 50 μm. (A) adapted with permission from Paxinos et al.[43]

reliable DREADD methods in NHPs has been challenging, and the work presented here builds on encouraging recent progress.[23–34]

The use of DREADDs in humans will require methods for the precise delivery of viral vectors to targeted brain regions, sufficient expression of DREADDs in neuronal populations, as well as DREADD-activating drugs that are acceptable for human use. Additionally, use of this technology in humans will benefit from the ability to validate *in vivo*, the location and success of virally mediated DREADD expression, which could be accomplished with DREADD-specific positron emission tomography (PET) scanning. While clozapine-*N*-oxide (CNO) was initially proposed as an ideal DREADD-activating drug with high affinity and selectivity for DREADD receptors and has been extensively used in rodent studies (for review, see Wess et al.[35]), recent pharmacokinetic evidence suggests that CNO has poor brain penetrance.[36,37] Additionally, studies in rodents, humans, and NHPs demonstrate that CNO can be back-metabolized into clozapine.[36–41] Because clozapine has high brain penetrance[36,42] and can activate DREADDs at low doses,[20,36] it has been suggested that the effects of CNO are mediated, at least in part, by clozapine.[36,37]

Here, in an effort to develop new treatments for pathological anxiety, as well as to further develop the framework for using DREADDs in NHPs, we (1) performed *ex vivo* immunohistochemical and autoradiographic studies to validate hM4Di expression and ligand binding to the receptor in the primate amygdala, (2) confirmed *in vivo*, with [^{11}C]-deschloroclozapine (DCZ) microPET imaging, successful viral infection, and transduction resulting in hM4Di amygdala expression, (3) established individualized dosing strategies for clozapine to limit off-target effects, and (4) implemented a within- and between-subjects experimental design to test whether DREADD-mediated inhibition of dorsal amygdala neurons would lead to a reversible decrease in anxiety-related behaviors. These studies provide important insights into the feasibility of using circuit-specific interventions to treat psychiatric illnesses that are not amenable to current treatments.

RESULTS

Establishing viral vector-mediated expression of hM4Di-HA in the rhesus amygdala

To demonstrate efficacy of the viral vector method, we performed experiments in two pilot animals with injections of AAV5-hSyn-HA-hM4Di into the amygdala. One animal (subject P1; see Table S1 for definition of subject identifiers) received bilateral 24 μL injections into the dorsal amygdala, and 36 days later the brain was perfused and collected for immunohistochemical analysis (chromogenic 3,3′-diaminobenzidine [DAB] staining and immunofluorescence). In one hemisphere, stereological methods (see Table S2 for details) were used in immunofluorescently labeled sections to estimate the total number of transduced neurons in the Ce (including both the lateral and medial divisions), as well as the basal nucleus (including the magnocellular and intermediate divisions; see Figure 1A). Approximately 27% of all neurons in the analyzed portions of the basal nucleus expressed hM4Di-HA, with dorsal regions showing relatively high density of hemagglutinin (HA) and NeuN co-labeling (see Figure 1B). This is in contrast to the Ce, where less than 2% of neurons expressed DREADDs, and co-labeling of HA and NeuN was sparsely distributed (see Figure 1B). The other hemisphere of subject P1 was used for electron microscopy analyses, which as previously published demonstrated robust expression of hM4Di-HA on the cell membrane.[23]

To assess receptor binding, another animal (subject P2) received a unilateral 24 μL injection of AAV5-hSyn-HA-hM4Di into the dorsal region of the amygdala, and 35 days after surgery the brain was flash frozen and coronally sectioned for *in vitro* autoradiography. As can be seen in Figures 2A and 2B, specific binding of [^{3}H]clozapine was

Please cite this article in press as: Roseboom et al., Evidence in primates supporting the use of chemogenetics for the treatment of human refractory neuropsychiatric disorders, Molecular Therapy (2021), https://doi.org/10.1016/j.ymthe.2021.04.021

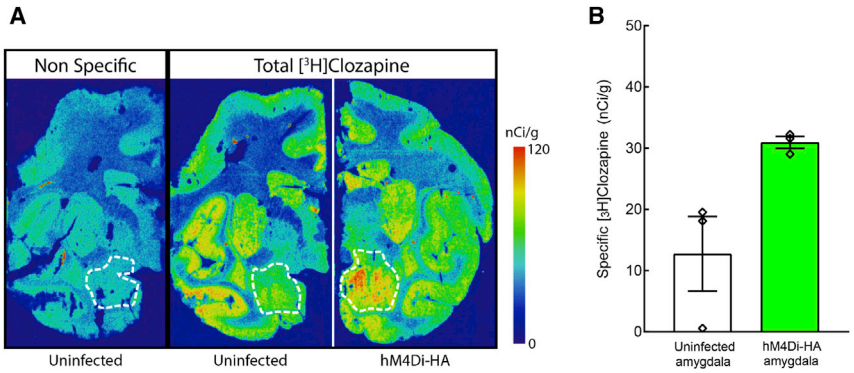

Figure 2. Autoradiographic demonstration of hM4Di-HA expression in the rhesus amygdala

(A) Autoradiograms from subject P2 unilaterally injected with AAV5-hSyn-HA-hM4Di (hM4Di-HA) into the amygdala, showing nonspecific and total [^{3}H]clozapine (3.5 nM) binding. The white dotted line depicts the amygdala boundaries. (B) Densitometric quantification of specific binding ([^{3}H] clozapine total binding – nonspecific: total binding was assessed in three coronal slices) in the viral-infected amygdala compared to the uninfected amygdala. Error bars represent +/- SEM.

2.4-fold greater in the hM4Di expressing amygdala (right hemisphere) compared to the uninjected amygdala (left hemisphere).

Determining clozapine dosing for DREADD experiments in rhesus monkeys

To establish a dose of clozapine that is without significant effects on anxiety-related behaviors such as freezing, we administered vehicle, 0.1 mg/kg, and 0.5 mg/kg clozapine IM (n = 5/group) prior to exposure to 30 min of the no-eye-contact (NEC) condition. A one-way ANOVA revealed a significant effect of dose on freezing behavior ($F_{2,12} = 7.97$, $p < 0.01$). The 0.5 mg/kg dose of clozapine significantly decreased the duration of freezing ($p < 0.01$), which was not the case at the 0.1 mg/kg dose (Figure 3). Similarly, there was a significant effect of dose on experimenter orient ($F_{2,12} = 5.25$, $p < 0.05$). The 0.5 mg/kg dose of clozapine significantly decreased the duration of time spent orienting toward the experimenter ($p < 0.05$), whereas this was not the case at the 0.1 mg/kg dose. There was no significant effect on the duration of locomotion ($F_{2,12} = 0.13$, $p = 0.88$).

Establishing individualized doses of clozapine for the DREADD behavioral experiment

While the previous clozapine dose ranging experiment established that the 0.1 mg/kg dose, on average, was without significant effects on freezing behavior, we observed individual variation in response to the 0.1 mg/kg dose. Therefore, to reduce the potential for intrinsic effects of clozapine on behavior, during subject selection we assessed the effects of 0.03 and 0.1 mg/kg clozapine on each animal's behavior to develop an individualized dosing strategy. For each pair of animals (control and experimental) the highest dose of clozapine that was without behavioral effects was chosen. The 0.03 mg/kg dose was selected for three of the pairs and the 0.1 mg/kg dose was selected for the remaining two pairs (of note, one pair of animals received only vehicle and 0.1 mg/kg clozapine during pre-testing).

In the four pairs of animals that received both doses of clozapine, plasma levels of clozapine and norclozapine demonstrated significant dose-dependent increases (clozapine, $t_7 = 8.49$, $p < 0.0001$; norclozapine, $t_7 = 6.11$, $p < 0.001$). The plasma clozapine levels (mean ± SEM) at the 0.03 mg/kg and 0.1 mg/kg doses were 4.8 ± 1.2 ng/mL and 16.6 ± 1.9 ng/mL, respectively. Similarly, plasma norclozapine levels were 0.34 ± 0.06 ng/mL and 0.89 ± 0.10 ng/mL, respectively. Plasma levels of CNO were below the detection limit of the assay. Additionally, these doses of clozapine significantly decreased NEC-induced plasma ACTH ($F_{2,14} = 6.88$; $p < 0.05$; Figure 4) and cortisol concentrations ($F_{2,14} = 4.60$; $p = 0.05$; Figure 4). Because of these effects on plasma ACTH and cortisol, these hormonal measures were not analyzed in the DREADD experiment. Also, because NEC-induced cortisol is a component of the AT score, we did not use this composite score in assessing the effects of DREADD-mediated amygdala inhibition.

Assessing hM4Di-HA expression in the experimental animals

The 5 monkeys that were selected as the experimental subjects received bilateral infusions of AAV5-hSyn-HA-hM4Di, with gadolinium as a contrast agent, targeted toward the dorsal amygdala region containing the Ce, as well as the dorsal aspects of the basal and accessory basal nuclei. After completion of each infusion, an MRI scan was acquired to visualize the infusate delivery region. Post-infusion scans were used to create a map indicating the infusion region that was overlapping and shared across the 5 subjects (Figure 5B). This revealed an overlap in gadolinium diffusion in the dorsal amygdala region, including the Ce and middle to dorsal aspects of the basal and accessory basal nuclei.

After behavioral testing, two experimental animals (subjects E2 and E3) and one unoperated animal (subject C1, which was not part of this study but had a similar prior experience with testing and clozapine dosing) underwent [^{11}C]-DCZ microPET scanning to assess *in vivo* hM4Di expression and localization. [^{11}C]-DCZ, a derivative of clozapine, has recently been shown to be an effective PET radioligand for visualizing DREADDs due to its high selectivity and specificity for the hM4Di receptor.[34] To quantitatively assess specific [^{11}C]DCZ binding, we derived distribution volume ratio (DVR) parametric images using the cerebellum as a nonspecific-binding reference region (see Figure S2).[44,45] Because of individual variation in brain [^{11}C]DCZ binding observed across the three animals, images were scaled such that the specific binding (i.e., DVR) in the prefrontal cortex was matched across the images. We then subtracted the aligned and scaled images of the control animal from each of the hM4Di-HA

Please cite this article in press as: Roseboom et al., Evidence in primates supporting the use of chemogenetics for the treatment of human refractory neuropsychiatric disorders, Molecular Therapy (2021), https://doi.org/10.1016/j.ymthe.2021.04.021

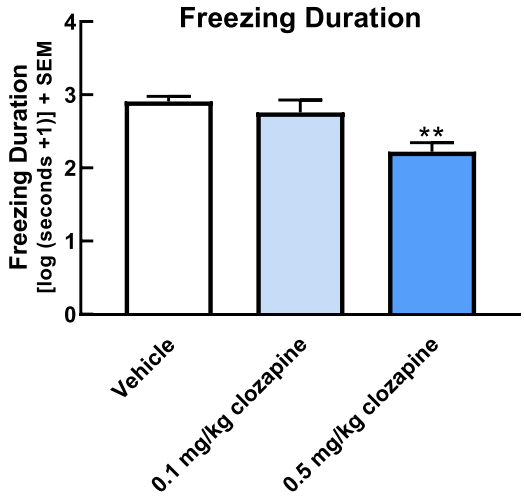

Figure 3. Effects of clozapine administration on freezing behavior during NEC

Log transformed freezing duration following administration of vehicle or two different doses of clozapine (n = 5/group). Compared to vehicle, there was a significant reduction in freezing duration following 0.5 mg/kg clozapine but not 0.1 mg/kg clozapine (**p < 0.01).

animals' images. Figure 6 depicts the average of these two difference images, overlaid on a template MRI, demonstrating a 40%–50% [^{11}C] DCZ signal increase in the amygdala region of the hM4Di-HA animals.

The brain from an additional experimental animal (subject E1) was used to quantify hM4Di-HA expression in the dorsal amygdala region of both the left and right hemispheres using stereological methods. This histological analysis focused on the regions of the amygdalae derived from the MRI images of gadolinium diffusion that overlapped across the 5 experimental subjects. Consistent with the overall pattern of expression observed in the tissue from subject P1, co-expression levels of NeuN and hM4Di-HA as assessed with immunofluorescence were greatest within the dorsal portions of the basal and accessory basal nuclei compared to lower levels in the Ce (see Figure 7). Focusing on these nuclei, co-labeling of neurons was counted in subsampled regions encompassing 200 × 200 × 10 μm volumes. These analyses of portions of the right and left amygdala revealed transduction efficiencies in the subsampled regions that varied, ranging up to 67% (refer to Figure S3 for further details). Additionally, some hM4Di-HA expression was observed in the dorsal region of the lateral nucleus, with much sparser expression in other amygdala nuclei. Outside of the amygdala, sparse cell-body labeling was also observed in the anterior hippocampus and ventral putamen. We also examined some projection sites of the amygdala to understand the extent to which DREADDs are anterogradely transported and expressed in the projections of infected cells. Consistent with this, chromogenic labeling of the HA-tag revealed discernible fibers in the bed nucleus of the stria terminalis, sublenticular extended amygdala, and lateral septum (Figure S4).

hM4Di-HA activation decreases anxiety-related freezing behavior in the NEC condition

Increased freezing is the prominent behavioral response occurring during the NEC condition. Using a 2 × 2 design, we examined clozapine-induced changes in freezing behavior (clozapine minus vehicle) across group (control versus hM4Di-HA) and session (pre versus postsurgical testing). Results demonstrated no significant main effect of group and no significant main effect of session. However, there was a significant group × session interaction ($F_{1,8}$ = 14.89, p = 0.0048), such that in hM4Di-HA animals, clozapine treatment produced a significant change in freezing duration after, as compared to before, viral vector infusion (p = 0.007; Figure 8). This was not the case in the control animals. We note an outlying data point in the hM4Di-HA group during the pre-testing period (diamond symbol; Figure 8) and when removing the pre and post data from this animal and its cage-mate control, the results remain significant (group × session interaction; $F_{1,6}$ = 12.09, p = 0.013). Because of the potential for individual differences in response to clozapine and because different doses of clozapine were used for different pairs of animals, we also performed an analysis residualizing the freezing durations with the plasma clozapine levels for all pre and post behavioral sessions. This analysis did not change the findings when the entire sample was included (group × session $F_{1,8}$ = 16.87, p = 0.0034) or when the outlying pair of animals was removed from the analysis (group × session $F_{1,6}$ = 9.18, p = 0.023). We also note that clozapine and norclozapine plasma levels did not significantly differ between the control and hM4Di-HA groups either prior to or after surgery.

Because we detected significant effects of hM4Di-HA activation on freezing during the NEC condition, we also examined the extent to which hM4Di-HA activation affected freezing during the Alone and Stare conditions during which freezing is much less prominent. An analysis of the clozapine-induced changes in freezing behavior (clozapine minus vehicle) across the three human intruder paradigm (HIP) conditions (Alone, NEC, and Stare) was restricted to the postsurgical data because data from the Stare condition were only collected during the postsurgical period. The results demonstrated a significant main effect of group such that the DREADD animals had an overall greater reduction in freezing behavior than controls across all conditions ($F_{1,8}$ = 10.63; p = 0.012). Also, there was a lack of a significant HIP condition × group interaction ($F_{2,16}$ = 1.93, p = 0.18), suggesting that hM4Di-mediated amygdala inhibition reduced freezing behavior across conditions. When examining each condition separately, hM4Di activation was associated with reductions in freezing (Alone, p = 0.073; NEC, p = 0.018; Stare, p = 0.0081). The results were unaffected when residualizing for plasma clozapine levels (group – $F_{1,8}$ = 19.61; p = 0.0022; HIP condition × group – $F_{2,16}$ = 0.76, p = 0.48).

We next assessed the effects of hM4Di-mediated amygdala inhibition on the prominent behaviors that occur during the Alone and Stare conditions. The analysis for the Alone condition compared clozapine-induced changes (clozapine minus vehicle) before and after surgery. Increases in coo vocalizations and locomotion commonly occur during the Alone condition, and neither of these were significantly

Please cite this article in press as: Roseboom et al., Evidence in primates supporting the use of chemogenetics for the treatment of human refractory neuropsychiatric disorders, Molecular Therapy (2021), https://doi.org/10.1016/j.ymthe.2021.04.021

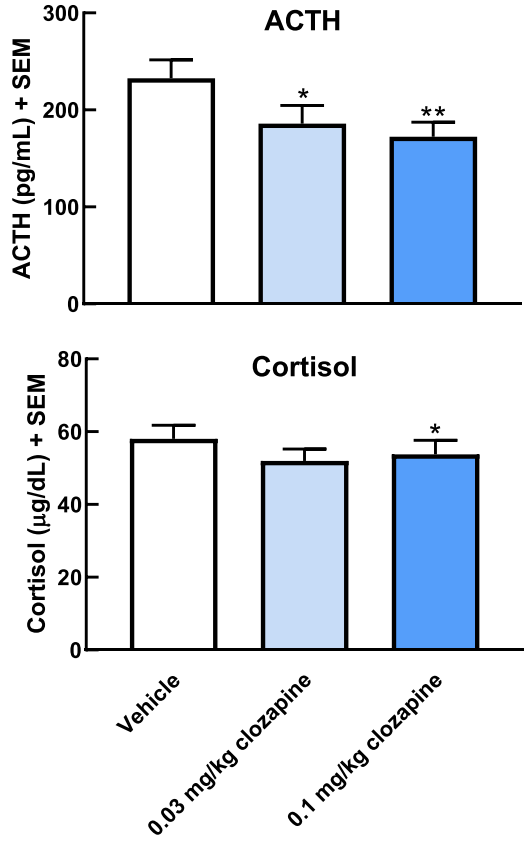

Figure 4. Effects of 0.03 mg/kg and 0.1 mg/kg clozapine on plasma ACTH and cortisol levels in animals selected for the DREADD behavioral experiment

As part of characterizing individual doses of clozapine, effects on ACTH (upper) and cortisol (lower) were assessed following administration of vehicle, 0.03, and 0.1 mg/kg clozapine to the same animals (n = 8). ACTH was significantly reduced by both doses, whereas significant reductions in cortisol occurred at the higher dose (*$p < 0.05$, **$p < 0.01$).

affected by clozapine-induced hM4Di activation. Bark vocalizations and experimenter-directed hostility are the prominent behaviors that are elicited by the Stare condition. Postsurgical data for the Stare condition (clozapine minus vehicle) revealed that these behaviors were unaffected by hM4Di-mediated amygdala inhibition.

DISCUSSION

In the present study, we demonstrate that activation of the inhibitory hM4Di in the dorsal amygdala with low dose clozapine significantly decreases NHP anxiety-related behavior. Autoradiographic studies validated that clozapine binds to hM4Di-HA receptors expressed in the amygdala, and immunohistochemical methods determined that neurons expressing these receptors were most prominently located in the dorsal regions of the basal and accessory basal nuclei. Advancing the translational utility of chemogenetics, we replicate the finding that [^{11}C]-DCZ microPET scanning can be used to visualize DREADD expression *in vivo*,[34] revealing selective binding in the viral vector targeted regions of the amygdalae.

Because clozapine has affinity for many endogenous receptors and is well known to have behavioral effects,[46,47] and because we observed individual differences in responses at low doses, we used an individually determined dosing approach in the DREADD experiment. The goal of the individualized approach was to identify the highest dose of clozapine that was without off-target behavioral effects. Animals were tested in pairs (experimental and control) and the same dose was selected for further experimentation in each pair. Thus, optimal and identical dosing was used for each member of each pair of animals. There was no significant difference in plasma levels between control and experimental subjects because the experimental animal and its paired control received the same dose of clozapine. Additionally, we used plasma levels in the behavioral analyses to control for any potential pharmacokinetic differences between animals.

The findings demonstrated a significant clozapine-induced decrease in freezing behavior in the hM4Di-HA subjects during NEC, a threat-related context in which the predominant response is to freeze. In addition to the effects observed during NEC, hM4Di activation also reduced freezing during the Alone and Stare conditions. No significant effects of DREADD activation were observed for other behaviors including coo or bark vocalizations, locomotion, or experimenter-directed hostility. The effects of hM4Di-induced amygdala inhibition on freezing are consistent with previous publications examining the effects of amygdala lesions on threat-related responses in NHPs and rodents.[19,48,49]

A previous study used clozapine and CNO to examine the impact of hM4Di-HA DREADD-mediated amygdala inhibition on anxiety-related behavior during the HIP in two young rhesus monkeys.[31] While no control group was included in the DREADD behavioral analyses, this study reported decreased drug-induced (CNO and clozapine) freezing during the HIP with no changes in vocalizations, which is consistent with our findings. In another study using CNO, DREADD-induced amygdala inhibition in adult rhesus monkeys resulted in reductions in amygdala-frontal cortex resting-state functional connectivity.[27] This finding is interesting in relation to our demonstration of a DREADD-induced reduction in threat-related freezing behavior as the circuit disruptions reported by Grayson et al.,[27] overlap with regions implicated in mediating primate threat-related anxiety.[7,50] This study also did not use a non-DREADD control group as a comparator, leaving open the possibility that the observed effects could be due to the intrinsic actions of CNO and/or its back metabolism to clozapine and not to DREADD activation per se.

In the present study, we used gadolinium as an MRI contrast agent during the viral vector infusion to intraoperatively observe the extent of the infusion. Previous studies utilizing gadolinium to monitor viral infusions have shown that *in vivo* assessment of gadolinium distribution can predict the distribution of protein expression resulting from AAV-mediated infection.[51,52] Consistent with this, our histochemical characterization of a DREADD behavioral study subject demonstrated considerable expression in the dorsal portions of the basal

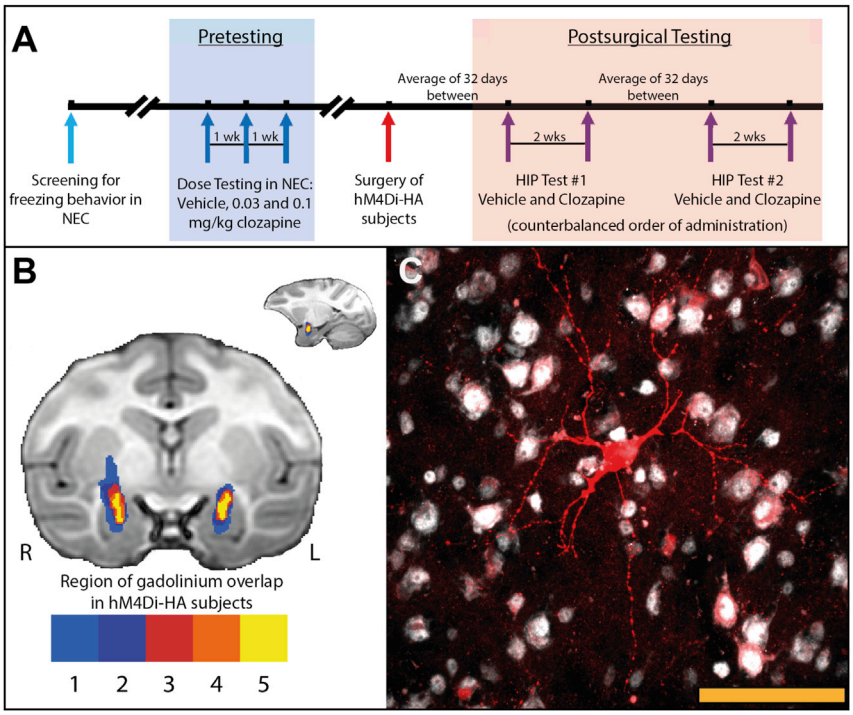

Figure 5. DREADDs experiment methods

(A) Timeline for behavioral testing of monkeys receiving AAV5-hSyn-HA-hM4Di (n = 5) and cage-mate controls (n = 5). (B) Overlap of the infused area across all subjects as assessed by the gadolinium signal detected with MRI. The colors represent the number of animals with gadolinium signal at each voxel. The overlap of the gadolinium injection clouds across all five experimental animals is depicted in yellow demonstrating consistent coverage of the dorsal amygdala region using the MRI-guided targeted injection procedure. (C) Neurons expressing hM4Di-HA in a section containing the accessory basal nucleus in a maximum intensity projection image at 40× integrated across the z stack; scale bar (yellow) represents 100 μm. Neurons are identified with NeuN in gray, and hM4Di-HA expression with HA immunoreactivity in red. Note, the neuron seen in center of the field of view is prominently expressing hM4Di-HA in its soma, as well as in its neuronal extensions.

and accessory basal nuclei. A similar expression pattern was observed in the pilot subject. While we assume that the expression is similar in the four additional experimental animals, this remains to be confirmed.

Based on the predominance of DREADD expression in the dorsal regions of the basal and accessory basal nuclei and the known functions of these nuclei, it is plausible that the infected neurons in these regions mediated the reductions in threat-related freezing behavior. The basal and accessory basal nuclei are primarily composed of glutamatergic projection neurons, along with a smaller population of GABAergic interneurons.[53–55] Because our DREADD construct utilized the synapsin promoter, both of these cell types were likely infected. The basal and accessory basal nuclei receive sensory input from the thalamus and the cortex, as well as higher order information from the hippocampus and PFC,[56,57] and send outputs to the Ce, BST, striatum, hypothalamus, hippocampus, and PFC.[58–61] Many rodent studies have demonstrated that these amygdala subregions are involved in modulating anxiety-related behavior.[61–68] For example, inhibition of basolateral projections to ventral hippocampus have been shown to decrease anxiety-related behaviors,[67] whereas inhibition of basolateral projections to the lateral division of the Ce have been shown to increase anxiety-related behaviors.[68] Furthermore, human imaging studies further implicate a role for basal, accessory basal, and lateral nuclei (considered together as the basolateral amygdala [BLA]) dysfunction in psychiatric disorders, as disruptions in BLA functional connectivity are observed in patients with generalized anxiety disorder.[69]

In addition to the considerable expression in the dorsal basal and accessory basal nuclei, a low level of DREADD expression was observed in the Ce. The Ce consists primarily of GABAergic neurons and is considered the major output nucleus of the amygdala.[70] In addition, our previous mechanistic and neuroimaging work has implicated the Ce as a key node in the neural network underlying the expression of AT.[71] It is conceivable that the modulation of a small number of neurons in the Ce is sufficient to induce alterations in behavior. Other work in NHPs has demonstrated that DREADD transduction levels as low as 3% of neurons in the dorsolateral PFC appears to be effective at influencing spatial working memory.[29] Thus, in addition to the probable contribution of the dorsal basal and accessory basal nuclei, it is possible that the small number of Ce neurons expressing hM4Di could be contributing to the behavioral effects observed here. Of further consideration, some hM4Di expression was observed in neurons located between the basal and accessory basal nuclei and the Ce. This is potentially important because the GABAergic neurons found in this region, which constitute the intercalated cell masses, act as an inhibitory gate for information flowing from the BLA to the Ce.[72,73]

The sparsity of Ce hM4Di expression found in the present study is consistent with data from other reports in primates using AAV2 or AAV5 infused into the amygdala.[27,52,74] Interestingly, in rodent studies, AAV5 has been successfully utilized to infect the Ce.[75–77] Other data from our laboratory (S.A.L.M. and N.H.K., unpublished data) suggests that various AAV vectors, specifically AAV8 and AAV9, also show scarce Ce infectivity in primates. Studies aimed at characterizing the role of the NHP Ce will require the identification of methods that more robustly infect NHP Ce neurons.

Overall, our findings demonstrate the utility of using DREADD technology in NHPs to investigate the neural circuitry underlying the expression of anxious behavior and further highlight the importance

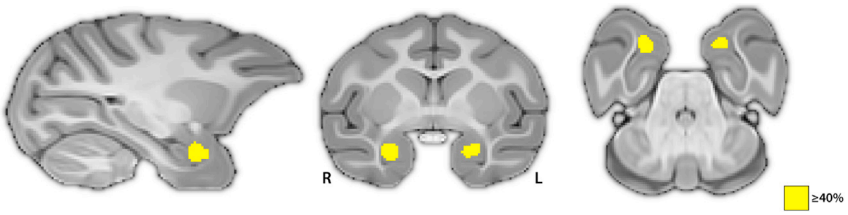

Figure 6. [^{11}C]DCZ binding in the amygdala demonstrates hM4Di-HA expression *in vivo*

The average difference (hM4Di-HA minus control) in [^{11}C]DCZ binding signal from two of the hM4Di-HA animals in the DREADDs behavioral experiment is overlayed on a rhesus monkey brain MRI template. The average difference image is thresholded at 40%. Greater binding is observed bilaterally in the amygdala, where the AAV5-hSyn-HA-hM4Di virus was infused and where gadolinium signal was observed across all five hM4Di-HA subjects. The peak difference in the right amygdala reached 53% greater binding signal in the hM4Di-HA animals. No other brain regions exceeded this threshold. See also Figure S2.

of the amygdala in threat-related responding. In future studies, chemogenetic technology could be similarly applied to functionally define the role of other cortical and subcortical components of the neural circuitry underlying primate anxiety. The implementation of chemogenetic technology in this NHP model sets the stage for the possibility of using DREADDs to identify and develop novel clinical interventions targeting specific cell types within specific regions of the neural circuits that underlie human pathological anxiety.

MATERIALS AND METHODS

Experimental model and subject details

Studies were performed using male and female rhesus monkeys (*Macaca mulatta*), with the gender composition and age ranges as described for each study in the methodological details below. Monkeys were housed and cared for at the Wisconsin National Primate Research Center and the Harlow Center for Biological Psychology on a 12-h light/dark cycle, in a temperature- and humidity-controlled vivarium. Procedures were performed using protocols that were approved by the University of Wisconsin Institutional Animal Care and Use Committee in compliance with the Guide for the Care and Use of Laboratory Animals published by the US National Institutes of Health.

Assessing behavioral effects of clozapine

Prior to beginning studies using the DREADD virus, we assessed whether low doses of clozapine administered to control subjects would impact the level of anxiety-like responding during the NEC condition of the HIP.[3,12,78] Using a between-subjects design (n = 5/grp; males, mean age at time of behavioral testing = 2.03 ± 0.07 years), monkeys were treated with either vehicle, 0.1 mg/kg clozapine, or 0.5 mg/kg clozapine. The solutions used for the 0.1 mg/kg and 0.5 mg/kg doses were prepared at a concentration of 0.2 mg/mL and 1 mg/mL, respectively, by dissolving the clozapine in DMSO and then diluting in 0.9% saline to a final DMSO concentration of 25%. The drug was administered as bilateral intramuscular (IM) injections at a volume of 0.5 mL/kg. Vehicle injected animals received 0.5 ml/kg of 25% DMSO in 0.9% saline. Drug or vehicle was administered 40 min prior to exposure to 30 min of NEC. The duration of freezing behavior, which was defined as a lack of movement for greater than 3 s, the duration of locomotion, which was defined as ambulation of one or more steps at any speed, and the duration of experimenter orient, which was defined as any non-hostile orienting behavior toward the experimenter, were recorded in s.

AAV5-hSyn-HA-hM4Di DREADDs subjects

The timeline for behavioral testing of subjects is shown in Figure 5A. To maximize the potential for observing the hypothesized decrease in freezing resulting from the DREADDs receptor activation, we initially screened monkeys with 10 min of NEC to identify and select mid- to high-level freezers. Of the 94 animals that were screened (47 males/47 females, mean age at time of screening 1.83 ± 0.08 years), 16 were then chosen to be tested for responsiveness to clozapine. Animals were tested using 10 min of Alone followed by 10 min of NEC following administration of vehicle, 0.03 mg/kg clozapine and 0.1 mg/kg clozapine. One pair of animals received only the 0.1 mg/kg dose of clozapine during the clozapine responsiveness testing. The solutions used for the 0.03 mg/kg and 0.1 mg/kg clozapine doses had concentrations of 0.06 mg/mL or 0.2 mg/mL, respectively, and were prepared and administered as described in the preceding section (assessing behavioral effects of clozapine). Drug or vehicle was administered 30 min prior to behavioral testing. At the conclusion of the test, blood was collected to assess the impact of clozapine on plasma ACTH and cortisol levels and measurement of plasma clozapine and norclozapine levels. All blood collections were done at the same time of day (range 8:43 AM–11:05 AM). To obtain plasma, we collected blood in EDTA tubes and immediately centrifuged them at 1,900 × g for 10 min at 4°C and collected the supernatant. Tests were separated by 1 week and the order was randomized. Animals that showed a pronounced clozapine-induced decrease in freezing during the NEC even at the low dose were not used further in the study. Ultimately, 10 animals were chosen for surgery or to serve as matched unoperated control subjects (6 males and 4 females, mean age at time of surgery = 2.19 ± 0.23 years). The clozapine testing procedure also determined the dose of clozapine used in the post-surgery testing. We chose the highest dose of clozapine that did not substantially affect freezing behavior in the NEC, which for two pairs of animals was 0.1 mg/kg and for the other three pairs was 0.03 mg/kg.

Post-surgical testing began approximately 32 days after surgery (see Figure 5A). The clozapine preparation and injection methods were the same as for the screening procedure. Drug or vehicle was administered 30 min prior to behavioral testing. Behavioral testing was performed using the HIP, which consisted of 10 min of Alone, 10 min of NEC, 5 min of Alone, 10 min of Stare, and ending with 15 min of Alone followed by blood collection for measurement of plasma

Please cite this article in press as: Roseboom et al., Evidence in primates supporting the use of chemogenetics for the treatment of human refractory neuropsychiatric disorders, Molecular Therapy (2021), https://doi.org/10.1016/j.ymthe.2021.04.021

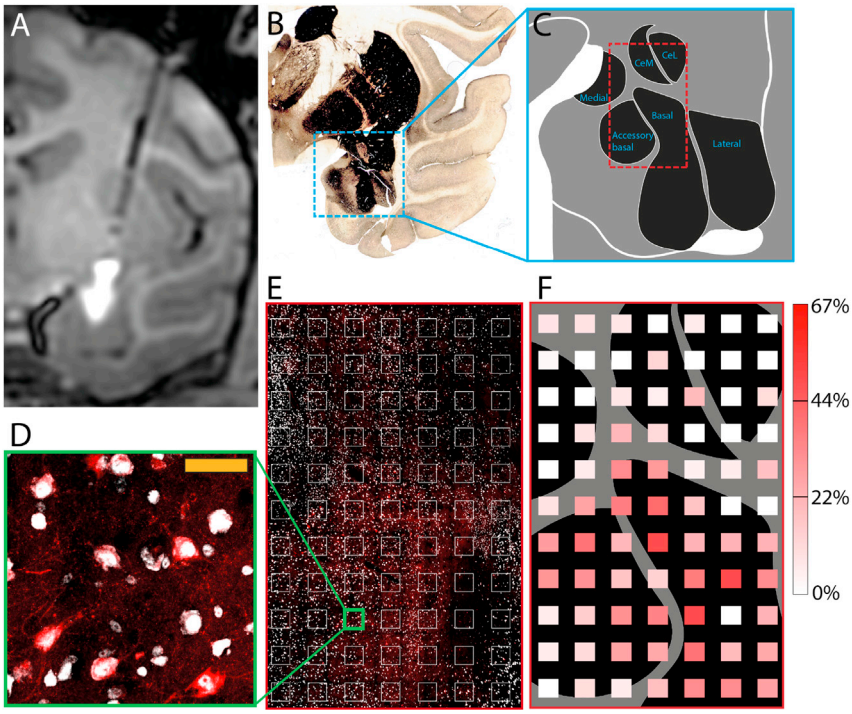

Figure 7. Quantification of hM4Di-HA expression in the amygdala

(A) Intraoperative MRI image of the gadolinium signal after the infusion into the dorsal amygdala of AAV5-hSyn-HA-hM4Di mixed with gadolinium. (B) Acetylcholinesterase staining of a tissue section containing the amygdala from subject E1, demonstrating considerable staining in the basal nucleus and a lack of staining in the central nucleus. (C) A depiction of the amygdala nuclei as derived from acetylcholinesterase staining. The box outlined in red represents the region of one of the sections that was used in the stereological analysis. (D and E) A 200 × 200 × 10 μm subregion within the accessory basal nucleus that was part of the stereological analysis (D), which is a magnification of the green square in (E); scale bar (yellow) represents 50 μm. Red fluorescence indicates HA immunoreactivity, and gray fluorescence indicates NeuN immunoreactivity. (E) A tissue section used for stereological assessment of the co-expression of HA (red) and NeuN (greyscale). White squares indicate subregions where co-expression was quantified. (F) A heatmap of the percent of neurons, identified with NeuN, that are co-expressing HA, reflecting the stereological analysis performed on the section depicted in (E). See also Figure S3.

clozapine and norclozapine levels. All blood collections were done at the same time of day (range 9:10 AM–11:07 AM). Subjects were tested with vehicle and either 0.03 mg/kg or 0.1 mg/kg clozapine based on the results from the screening tests. Postsurgical behavioral testing was performed with randomized drug and vehicle administration separated by at least 2 weeks. Subjects received a second round of testing approximately 32 days later with counterbalanced drug and vehicle administration, again separated by at least 2 weeks. Prior to statistical analysis, the results were averaged across the two rounds of testing.

The HIP assesses monkeys in three different contexts eliciting different defensive responses. The HIP begins with the Alone condition, during which a monkey is separated from its cage-mate and is placed into a test cage by itself. This context typically elicits separation behaviors such as coo-vocalizations and increases in locomotion. The Alone condition is followed by the NEC condition wherein a human intruder enters the room and presents her/his profile to the monkey, while avoiding direct eye contact. Responses to this potentially threatening situation include increases in freezing, decreases in locomotion, and decreases in coo vocalizations. The final context is the Stare condition, during which the intruder reenters the room and stares directly at the monkey, eliciting hostile behaviors directed toward the intruder (i.e., bark vocalizations and experimenter-directed hostility).

Assessing neuroendocrine effects of clozapine

To examine the effects of clozapine dose on HPA axis function following 10 min of Alone and 10 min of NEC exposure, we assessed plasma levels of cortisol and ACTH.

ACTH assay

Plasma samples were assayed for ACTH using the MD Biosciences (Oakdale, MN, USA) enzyme-linked immunosorbent assay (ELISA) following the manufacturer's instructions. Samples were assayed in duplicate. The inter-assay CV percentages were calculated for a low and a high control sample. The low control had an average value of 41.7 ± 0.8 pg/mL and a CV percentage of 9.0, and the high control had an average value of 249.4 ± 4.2 pg/mL and a CV% of 7.8. The limit of detection defined by the lowest standard was 5 pg/mL.

Cortisol assay

Plasma samples were assayed for cortisol in duplicate using the MP Biomedicals (Solon, OH, USA) Immuchem coated tube radioimmunoassay. The intra-assay CV percentage was 4.9 and the inter-assay CV percentage was 9.8. The detection limit defined by the lowest standard was 1 μg/dL.

Assessing plasma levels of clozapine and its metabolites

Plasma levels of clozapine and its metabolites norclozapine and CNO were measured using HPLC coupled with mass spectroscopy as previously described.[30] The plasma aliquots used were collected at the conclusion of the behavioral tests. A Nexera XR HPLC (Shimadzu, Kyoto, Japan) coupled with a QTRAP 6500 (SCIEX, Redwood City, CA, USA) was used to acquire data that was analyzed with Analyst 1.6 (SCIEX).

Surgical procedures

Trajectory guide base placement and intraoperative MRI

The placement of the trajectory guide bases followed published methods[79,80] that were modified to target the dorsal amygdala

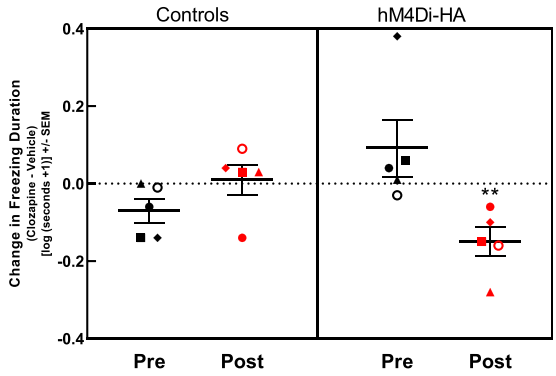

Figure 8. DREADD-induced change in anxiety-related behavioral response

The clozapine-induced change in freezing duration (clozapine-vehicle) occurring during the NEC component of the HIP for the hM4Di-HA and control animals. The five different symbols each identify an hM4Di-HA subject and its cage-mate control. Symbols in black represent the difference between clozapine and vehicle at baseline prior to surgery (pre). Symbols in red represent the difference between clozapine and vehicle after hM4Di-HA expression that is averaged across the two rounds of testing (post). A significant group by session (pre/post) interaction was observed ($F_{1,8} = 14.89$, $p < 0.01$). Post hoc testing revealed a significantly greater decrease in freezing for the hM4Di-HA animals post compared to pre (**$p < 0.01$), whereas the control animals did not significantly differ post compared to pre.

following procedures described in supplemental methods section of two previous publications[52,74] with slight modifications. To cover as much of the dorsal amygdala (Ce) and dorsal aspects of the basal and accessory basal nuclei) as possible while minimizing infection of the surrounding tissue, one 24 μL infusion was performed per hemisphere. In an effort to maximize coverage of the dorsal amygdala, the 24 μL was injected over multiple infusions with adjustments made to injector depth based on information obtained from the intraoperative MRI scans collected between infusions. As can be seen in Figure 5B, this ensured that the animals all received the DREADDs virus in an overlapping region of the dorsal amygdala.

Before the procedure, the animals were anesthetized with ketamine (up to 20 mg/kg, IM), prepared for surgery, and then placed in an MRI compatible-stereotaxic frame. The animals were intubated and received isoflurane anesthesia (1%–3%, intratracheal) with 1%–1.5% O_2 administered during induction. Atropine sulfate (0.01–0.4 mg/kg, IM) was administered to depress salivary secretion, and buprenorphine (0.01–0.03 mg/kg, IM, repeated every 6–12 h) was given for analgesia. To maintain fluids and electrolytes, Plasmalyte (up to 10 mg/kg/h, intravenous [i.v.]) was administered. Cefazolin (20–25 mg/kg, IM or i.v.) was administered as a prophylactic antibiotic 1 day prior to the surgery. Cefazolin was also administered immediately prior to surgery and then every 6 h while under anesthesia. All drugs and treatments were given in consultation with veterinary staff. Vital signs (heart rate, respiration, oxygen saturation, and end tidal CO_2) were continuously monitored. Body temperature was monitored during the surgical and MRI procedure and maintained in the MRI by wrapping the animals for warmth while incorporating a hot water heating device within the wrap.

Cannula trajectory planning and insertion

Cannula trajectory planning was carried out in the MRI suite under anesthesia as previously described.[74] The infusion line was primed with a loading line solution that was identical to the virus suspension solution (Dulbecco's phosphate-buffered saline [D-PBS] without Ca^{2+} or Mg^{2+} [GIBCO, Thermo Fisher Scientific, Waltham, MA, USA] containing 0.001% F68 surfactant [GIBCO, Thermo Fisher Scientific]), and the cannula was loaded with the DREADDs viral vector and the MR visible marker Gadobenate dimeglumine (Gd, MultiHance; Bracco Diagnostics, Monroe Township, NJ, USA). The pilot subject and four out of the five experimental subjects had a 100 mm length valve tip cannula (Engineering Resources Group, Pembroke Pines, FL, USA) with a fused silica cannula having a polyimide tubing tip that was sealed with a retractable glass fiber stylet. Its dimensions were as follows: tip outer diameter (OD) = 0.40 mm, inner diameter (ID) = 0.345 mm, length = 3.0 mm; shaft OD = 0.67 mm, ID = 0.45 mm, length = 97.0 mm from ferrule; and stylet OD = 0.275 mm. One subject had a 100 mm length cannula (Engineering Resources Group) with a fused silica single-end port cannula with OD = 0.67 mm and ID = 0.45 mm.

After the pressure in the infusion line was stabilized, the cannula was introduced into the brain, advancing the remote introducer at approximately 10–15 mm/min. The cannula was advanced two-thirds of the measured depth toward the target for partial insertion, and another targeting 3D T1W MRI was performed to confirm the correct trajectory and calculate the remaining distance from cannula tip to target. Once confirmed, the cannula was advanced to its final position and the stylet was retracted. When the pressure reading on the infusion pump controller system stabilized, the infusion began.

The infusate consisted of AAV5-hSyn-HA-hM4Di suspended in a solution identical to the loading line solution described above. To facilitate *in vivo* MRI visualization of the infusion, we mixed Gd with the viral vector at a final concentration 0.66 mM. In the pilot subject used for autoradiographic experiments, a total volume of 24 μL was infused unilaterally into the right dorsal amygdala region at a steady rate of 1 μL/min. In each of the five DREADDs behavioral experiment subjects, a total volume of 24 μL per hemisphere was bilaterally infused into the dorsal amygdala region at a steady state rate of 1 μL/min, except for one experimental monkey where the infusion into the right hemisphere was 3 μL/min to improve cannula flow possibly due to a clogged injector. After each infusion, another 3D MRI scan was reacquired for a qualitative visualization of the volumetric infusate delivery region. This sequence provides sensitivity to the contrast-enhanced infusate and sufficient gray/white contrast for easy identification of the infusion's anatomical location. These post infusion scans were used to create the infusion overlap image in Figure 5B. After the infusions were complete, the animal was transported back to the surgical suite. To reduce intracranial pressure and prevent brain swelling, we gave mannitol (up to 2.0 g/kg, i.v.) as needed. The trajectory guides were removed,

Please cite this article in press as: Roseboom et al., Evidence in primates supporting the use of chemogenetics for the treatment of human refractory neuropsychiatric disorders, Molecular Therapy (2021), https://doi.org/10.1016/j.ymthe.2021.04.021

and the incision was closed in layers before the animal was allowed to recover from anesthesia. Animals were given buprenorphine twice on the day following the surgery (0.01–0.03 mg/kg, IM). Cefazolin (20–25 mg/kg, IM or i.v.) or cephalexin (20–25 mg/kg, oral [PO]) was given twice daily for 5 days after surgery to prevent infection. The animals were allowed to recover, and testing did not commence until 28 to 35 days (average 32 days) after surgery.

Viral vectors

Monkeys received infusions of the DREADD viral vector AAV5-hSyn-HA-hM4Di obtained from the Boston Children's Hospital Viral Core Facility (Boston, MA, USA). The lot of virus used for the pilot subject had a titer of 6.95×10^{13} genome copies/mL, and the lot of virus used for the five experimental subjects had a titer of 6.28×10^{13} genome copies/mL. The construct plasmid map (pOTTC1484, Addgene, Watertown, MA, USA) is shown in Figure S1.

Validation of hM4Di-HA expression *ex vivo*

[^{3}H]Clozapine autoradiography

Autoradiography with [^{3}H]clozapine was used to demonstrate DREADD ligand binding in tissue sections obtained from the amygdala. 35 days following surgery, subject P2 was euthanized, the brain was removed, and the region containing the amygdala was cut coronally into a 21 mm thick slab that was then flash frozen in chilled isopentane (Thermo Fisher Scientific) maintained on dry ice. The tissue was then sectioned at 20 μm thickness and mounted onto Superfrost Plus microscope slides (Thermo Fisher Scientific) and stored at −80°C until use. For the assay, sections from the left and right hemisphere were matched in the coronal plane using acetylcholinesterase (AChE), a cholinergic marker that can identify nuclei within the amygdala.[43,81] Autoradiography using [^{3}H]clozapine was then performed following a published protocol described in detail in the supplemental methods section accompanying a previous publication starting with the preincubation step.[36] The image generated by the phosphorimager (Typhoon, FLA 7000, GE Healthcare, Piscataway, NJ, USA) was quantified using Multi Gauge v.3 software (Fuji Photo Film, Tokyo, Japan) by drawing a region of interest around the amygdala on the uninjected left hemisphere and the injected right hemisphere. Values were averaged and expressed as nCi/g with the use of carbon-14 standards (American Radiolabeled Chemicals, St. Louis, MO, USA) exposed and imaged on the same phosphor screen as the experimental slides. For each hemisphere, the specific [^{3}H]clozapine binding in the amygdala was obtained by subtracting the non-specific signal obtained in the presence of excess cold clozapine (100 μM) from the total [^{3}H] clozapine signal. Three tissue sections per hemisphere were used for the total [^{3}H] clozapine binding condition, while one tissue section per hemisphere was used for the non-specific binding condition.

Immunohistochemical procedures

HA-tag expression

Time between surgery and necropsy was 36 days for subject P1 and 434 days for subject E1. Animals were euthanized by transcardial perfusion with heparinized PBS at room temperature followed by fixation with 4% paraformaldehyde (PFA) in PBS at 4°C. In the case of subject P1, which was also used for electron microscopy studies, perfusion was performed using ice-cold, oxygenated Ringer's buffer followed by 4% PFA containing 0.1% glutaraldehyde in 0.2 M phosphate buffer, pH 7.4. Brains were removed and fixation was continued in the perfusion solution overnight at 4°C. The brains were placed in a brain block and cut into slabs that were subsequently processed through increasing concentrations of sucrose –10%, 20%, and 30%. The approximately 14 mm thick tissue slab containing the amygdala was frozen and cut at 40 μm on a cryostat (CryoStar NX50, Thermo Fisher Scientific). Tissue sections were stored in cryoprotectant (40 mM potassium phosphate/11 mM sodium phosphate buffer, pH 7.2, containing 30% ethylene glycol and 30% sucrose) at −20°C until use.

To observe hM4Di-HA expression within the amygdala, as well as its putative projection sites, we performed chromogenic labeling of HA-tag. Tissue sections were washed overnight with PBS to remove cryoprotectant, and all subsequent incubations were carried out at room temperature in PBS containing 0.3% Triton X-100. Three 5-min washes with PBS were performed in between each incubation step. To block endogenous peroxidase activity, we first incubated tissue sections in PBS containing 6% hydrogen peroxide for 30 min. Sections were then blocked in 5% normal goat serum (Cat # S-1000; Vector Laboratories, Burlingame, CA, USA) for 1 h. This was followed by an overnight incubation with a 1:400 dilution of rabbit monoclonal HA-tag antibody (C29F4, Cat # 3724; Cell Signaling Technology, Danvers, MA, USA), and a 1 h incubation with a 1:250 dilution of peroxidase-conjugated goat anti-rabbit immunoglobulin G (IgG) secondary antibody (Cat #PI-1000; Vector Laboratories). A 2-min incubation with ImmPACT DAB peroxidase substrate (Cat # SK-4105; Vector Laboratories) was then used for visualization. Sections were mounted on Superfrost Plus microscope slides, which were air-dried, dehydrated in 95% and then 100% ethanol, and placed in xylene for 5 min before coverslipping with DPX mounting medium. Images were captured using a DM6000B light microscope (Leica Microsystems, Buffalo Grove, IL, USA).

To identify neurons that were expressing hM4Di-HA, we performed immunofluorescent co-labeling of HA-tag and neuronal nuclei (NeuN; Figure 5C). Tissue sections were washed overnight with PBS to remove cryoprotectant, and all subsequent incubations were carried out at room temperature in PBS containing 0.3% Triton X-100. Three 5-minute washes with PBS were performed in between each incubation step. Tissue sections were first blocked in 5% normal goat serum (Cat # S-1000; Vector Laboratories, Burlingame, CA, USA) for 1 h. This was followed by an overnight incubation with a 1:400 dilution of rabbit monoclonal HA-tag antibody (C29F4, Cat # 3724; Cell Signaling Technology, Danvers, MA, USA), and a 1-h incubation with a 1:250 dilution of Alexa Fluor 488 conjugated goat anti-rabbit secondary antibody (Cat # A11008; Thermo Fisher Scientific). Tissue sections were then blocked in 5% normal donkey serum (Cat # 017-000-121; Jackson ImmunoResearch, Laboratories, West Grove, PA, USA). This was followed by an overnight incubation with a 1:2,000 dilution of mouse monoclonal NeuN antibody (clone A60, Cat # MAB377; MilliporeSigma, Darmstadt, Germany), and a

1 h incubation with a 1:250 dilution of Alexa Fluor 647 conjugated donkey anti-mouse secondary antibody (Cat # A31571; Thermo Fisher Scientific). Cellular nuclei were stained using a 1:10,000 dilution of 4',6-diamidino-2-phenylindole (DAPI) for 5 min. Sections were mounted on Superfrost Plus microscope slides using ProLong Gold Antifade Mountant (Cat # P36930; Thermo Fisher Scientific).

Imaging and stereological quantification of expression

For subject P1, 1:15 coronal sections through the central nucleus, or 1:30 coronal sections through the basal nucleus, were sampled for analysis of HA-tag and NeuN co-expression. For subject E1, 1:10 coronal sections through the amygdala were sampled for analysis of HA-tag and NeuN co-expression. Sections immediately adjacent to these were processed for AChE, a cholinergic marker that was used to identify nuclei within the amygdala.[43,81] Fluorescent image stacks were acquired using a A1R-Si+ confocal microscope (Nikon Instruments, Melville, NY, USA) with a pan fluor 40× oil objective (1.30 N.A.) and Nikon NIS-Elements software. Section thickness was measured by focusing on the top of each tissue section, refocusing to the bottom of the tissue section, and then measuring the difference in Z axis. All sections were imaged using the same acquisition settings, including magnification, laser power, camera gain, offset, pinhole size, and scan speed.

To evaluate neuronal expression of HA-DREADDs, we accomplished standard unbiased stereological counting of HA and NeuN immunopositive cells with the optical fractionator workflow in Stereo Investigator software (MBF Bioscience, Williston, VT). For further details concerning the stereological parameters used, see Table S2. Counting was performed by a single trained investigator.

Pilot studies were used to determine the appropriate counting parameters, such that there would be a sufficient number of neurons in each counting frame to allow for meaningful interpretation of percentage of neurons expressing hM4Di-HA in a given subsampled region. Cells that were immunoreactive for NeuN and HA-tag were identified using the soma as the counting target. Cells with a well-defined soma and nucleus were counted if they were within or intersecting with the dissector frame and not intersecting with lines of exclusion.

[^{11}C]DCZ radiosynthesis

The [^{11}C]deschloroclozapine was synthesized similar to published methods[34] with modifications. The radiolabeling synthon, [^{11}C]methyl triflate was produced using the gas phase method, starting with the production of [^{11}C]methane via the $^{14}N(p,\alpha)^{11}C$ nuclear reaction using a 90/10 H_2/N_2 target.[82] The [^{11}C]methane was converted to [^{11}C]methyl iodide through gas phase iodination with iodine vapor in a heated quartz tube using a recirculation process.[83] [^{11}C]MeI was then passed through a heated glass tube containing silver triflate for the production of [^{11}C]methyl triflate.[82] The [^{11}C]MeOTf was slowly bubbled into a reaction vial containing 0.2 mg 11-(1-Piperazinyl)-5*H*-dibenzo[*b*,*e*][1,4]diazepine precursor (Tocris, Bio-Techne, Minneapolis, MN, USA) and 0.3 mL anhydrous MeCN. The radiolabeling reaction occurred at room temperature for 5 min, after which 0.5 mL mobile phase was added to the vial and the entire solution injected onto the semi-preparative high-performance liquid chromatography (HPLC) system. The semi-preparative HPLC system consists of a Waters 515 HPLC pump (5 mL/min), Waters 2489 UV Detector (254 nm), Phenomenex Gemini NX C-18 column (250 mm × 10 mm), and a mobile phase composed of MeCN/H_2O/Et_3N (40/60/0.1%). The peak corresponding to [^{11}C]DCZ was collected and diluted in 60 mL water and trapped on a tC18 light cartridge (Waters, Milford, MA, USA), which was then rinsed with 10 mL 0.002N HCl. The [^{11}C]DCZ compound was then eluted from the cartridge using 0.5 mL EtOH and 10 mL 0.9% sodium chloride, USP through a Millex-FG membrane filter (MilliporeSigma, Darmstadt, Germany). The purity of the tracer was verified using a Phenomenex Luna C18 column (200 mm × 4.6 mm) and mobile phase of MeCN/H_2O/Et_3N (40/60/0.1%) with a flow rate of 2 mL/min. No radiochemical or chemical impurities were observed. The specific activity was 29.3 ± 15.3 mCi/nmol at end of synthesis (n = 4).

PET scanning

The subjects were anesthetized with ketamine (15 mg/kg, IM), given atropine sulfate (0.04 mg/kg, IM) to depress salivary secretion, intubated and given isoflurane anesthesia (1%–1.5%, IT), and placed in the Focus 220 microPET scanner in the prone position with the head facing downward and secured in a custom-made head holder. Throughout the experimental procedure vital signs (heart rate, respiration, oxygen saturation, end tidal CO_2, and body temperature) were continuously monitored. To maintain fluids and electrolytes, Plasmalyte (up to 10 mg/kg/hr, i.v.) was administered. A transmission scan was acquired for 518 s using a ^{57}Co rotating rod source to correct for the scatter and attenuation of radiation in the tissue. The PET scan was initiated with the injection of the [^{11}C]DCZ (n = 4; 4.85 mCi ± 0.23 mCi; 0.12 ± 0.06 μg DCZ). The list mode emission data was acquired for a total of 90 min and binned into a time series of 22 frames: 2 × 1 min, 4 × 2 min, 16 × 5 min. The PET data were reconstructed using filtered back-projection and a ramp filter into a matrix size of 128 × 128 × 95 with voxel dimensions of 0.959 mm × 0.959 mm × 0.796 mm. We note that four animals were scanned, two with AAV5-hSyn-HA-hM4Di in amygdala, one with AAV5-hSyn-HA-hM3Dq in amygdala, and one uninjected control. The data from the hM3Dq subject was not used in this study.

[^{11}C]DCZ binding image analysis

A parameter representing radioligand-receptor binding was calculated to serve as an index of neuroreceptor density. The DVR was estimated from the microPET time series for each voxel in this parametric image. The DVR images were calculated using the SRTM2 algorithm[44,45] and the cerebellar gray matter as the reference region of negligible specific ligand-receptor binding. The DVR images were spatially transformed into a common T1-weighted MRI template space made from 592 rhesus monkeys[7] and blurred with a 2 mm FWHM smoothing kernel using Advanced Normalization Tools (ANTs[84,85]). For the purpose of visualizing the presence of the hM4Di in the injected regions, the [^{11}C]DCZ DVR images were then scaled such that the specific binding in the prefrontal cortex was matched across the images. This was done to normalize for

overall global differences in DCZ-specific receptor expression across subjects, and the prefrontal cortex was selected because this region revealed the highest and most uniform values of [^{11}C]DCZ DVR across subjects. The image from the control subject was then subtracted from each of the hM4Di DREADDs subjects and the average of these two difference images was then calculated using FSL (FMRIB Software Library).

Quantification and statistical analysis

Autoradiographic data obtained from the [^{3}H]clozapine binding assay were compared between the uninjected left hemisphere and the injected right hemisphere using a two-tailed unpaired t test. In the initial dose response study to assess the effects of 0.1 mg/kg and 0.5 mg/kg clozapine on freezing, locomotion, and experimenter orient during NEC, the durations were transformed ($\log_{10}+1$) and then analyzed by ANOVA, followed by Dunnett's multiple comparison test comparing results from the two clozapine doses to vehicle. To analyze the plasma ACTH and the cortisol data from the 8 animals that received vehicle and both the 0.03 mg/kg and 0.1 mg/kg doses of clozapine, we used repeated-measures ANOVAs. *Post hoc* analysis was done with a Dunnett's multiple comparison test comparing the two doses of clozapine to vehicle. In these same 8 animals, to compare plasma clozapine and norclozapine levels that resulted from the 0.03 mg/kg and 0.1 mg/kg doses of clozapine, paired two tailed t tests were performed. To analyze the behavioral data from the hM4Di-HA study, we transformed averaged freezing and locomotion duration ($\log_{10}+1$) and square root transformed the averaged cooing frequency. Results from the vehicle condition were subtracted from the clozapine condition and the difference was analyzed using a two-way repeated-measure ANOVA. In an additional analysis, the freezing data were residualized for plasma clozapine concentration and then analyzed with a two-way repeated-measure ANOVA. *Post hoc* analysis was performed using Sidak's multiple comparison test. To compare plasma clozapine and norclozapine levels between the Control and hM4Di-HA DREADDs groups during postsurgical testing, we averaged the values obtained after the two HIP tests and compared them using unpaired two tailed t tests. All statistical testing was performed using either Prism v. 8.1 (GraphPad Software, San Diego, CA, USA) or IBM SPSS Statistics v. 25 (IBM, Armonk, NY, USA). Graphical representations of the data were prepared using Prism.

SUPPLEMENTAL INFORMATION

Supplemental information can be found online at https://doi.org/10.1016/j.ymthe.2021.04.021.

ACKNOWLEDGMENTS

We thank the personnel of the Harlow Center for Biological Psychology, the HealthEmotions Research Institute, the Waisman Laboratory for Brain Imaging and Behavior, the Wisconsin National Primate Research Center, the Wisconsin Institutes for Medical Research, K. Brunner, W. Block, E. Brodsky, A. Alexander, M. Emborg, E. Fekete, D. French, M. Rabska, and H. VanValkenberg. Confocal microscopy was performed at University of Wisconsin-Madison (UW) Biochemistry Optical Core, which was established with support from the UW Department of Biochemistry Endowment. This work was supported by NIH grant R01-MH046729 to N.H.K., the Waisman Center (P30-HD003352), and the NIDA Intramural Research Program (ZIA000069). Research reported in this publication was also supported in part by the Office of the Director, National Institutes of Health under award number P51OD011106 to the Wisconsin National Primate Research Center, University of Wisconsin-Madison. In addition, this research was conducted in part at a facility constructed with support from Research Facilities Improvement Program grant numbers RR015459-01 and RR020141-01. The content is solely the responsibility of the authors and does not necessarily represent the official views of the National Institutes of Health. Preliminary versions of this work were presented in poster form at the Society for Neuroscience meeting in San Diego, CA, November 3–7, 2018, and the Society of Biological Psychiatry meeting in Chicago, IL, May 16–18, 2019.

AUTHOR CONTRIBUTIONS

N.H.K., A.S.F., P.H.R., S.A.L.M., J.A.O., and M.M. conceptualized the study. N.H.K. oversaw the study. J.A.O., V.R.E., M.E.O., and M.K.R. performed the surgeries. P.H.R. performed the plasma endocrine assays, M.A.B. determined plasma clozapine levels and J.L.G. performed the *in vitro* autoradiography assays. M.K.R. and V.R.E. performed the behavioral data collection. P.H.R. and J.A.O. analyzed the behavioral data and S.A.L.M. performed the immunohistochemical microscopy and stereological analyses. A.H.D. and B.T.C. synthesized the PET ligand [^{11}C]-DCZ and aided in analysis of PET imaging data. P.H.R., S.A.L.M., J.A.O., and N.H.K. wrote the paper. All authors provided feedback.

DECLARATION OF INTERESTS

N.H.K. currently receives research support from the National Institute of Mental Health; serves as a consultant to CME Outfitters, the Pritzker Neurospsychiatric Disorders Research Consortium, Skyland Trail Advisory Board, and the Institute of Early Adversity Research External Scientific Advisory Board at the University of Texas – Austin; is a shareholder in Seattle Genetics; has served as co-editor of Psychoneuroendocrinology, and currently serves as Editor-in-Chief of The American Journal of Psychiatry. All other authors report no biomedical financial interests or potential declarations of interest.

REFERENCES

1. Kessler, R.C., Aguilar-Gaxiola, S., Alonso, J., Chatterji, S., Lee, S., Ormel, J., Ustün, T.B., and Wang, P.S. (2009). The global burden of mental disorders: an update from the WHO World Mental Health (WMH) surveys. Epidemiol. Psichiatr. Soc. *18*, 23–33.
2. Kessler, R.C., Ruscio, A.M., Shear, K., and Wittchen, H.U. (2010). Epidemiology of anxiety disorders. Curr. Top. Behav. Neurosci. *2*, 21–35.
3. Fox, A.S., Shelton, S.E., Oakes, T.R., Davidson, R.J., and Kalin, N.H. (2008). Trait-like brain activity during adolescence predicts anxious temperament in primates. PLoS ONE *3*, e2570.
4. Kalin, N.H., Shelton, S.E., Fox, A.S., Oakes, T.R., and Davidson, R.J. (2005). Brain regions associated with the expression and contextual regulation of anxiety in primates. Biol. Psychiatry *58*, 796–804.
5. Oler, J.A., Fox, A.S., Shelton, S.E., Rogers, J., Dyer, T.D., Davidson, R.J., Shelledy, W., Oakes, T.R., Blangero, J., and Kalin, N.H. (2010). Amygdalar and hippocampal substrates of anxious temperament differ in their heritability. Nature *466*, 864–868.

6. Alisch, R.S., Chopra, P., Fox, A.S., Chen, K., White, A.T., Roseboom, P.H., Keles, S., and Kalin, N.H. (2014). Differentially methylated plasticity genes in the amygdala of young primates are linked to anxious temperament, an at risk phenotype for anxiety and depressive disorders. J. Neurosci. *34*, 15548–15556.
7. Fox, A.S., Oler, J.A., Shackman, A.J., Shelton, S.E., Raveendran, M., McKay, D.R., Converse, A.K., Alexander, A., Davidson, R.J., Blangero, J., et al. (2015). Intergenerational neural mediators of early-life anxious temperament. Proc. Natl. Acad. Sci. USA *112*, 9118–9122.
8. Roseboom, P.H., Nanda, S.A., Fox, A.S., Oler, J.A., Shackman, A.J., Shelton, S.E., Davidson, R.J., and Kalin, N.H. (2014). Neuropeptide Y receptor gene expression in the primate amygdala predicts anxious temperament and brain metabolism. Biol. Psychiatry *76*, 850–857.
9. Shackman, A.J., Fox, A.S., Oler, J.A., Shelton, S.E., Davidson, R.J., and Kalin, N.H. (2013). Neural mechanisms underlying heterogeneity in the presentation of anxious temperament. Proc. Natl. Acad. Sci. USA *110*, 6145–6150.
10. Fox, A.S., Oakes, T.R., Shelton, S.E., Converse, A.K., Davidson, R.J., and Kalin, N.H. (2005). Calling for help is independently modulated by brain systems underlying goal-directed behavior and threat perception. Proc. Natl. Acad. Sci. USA *102*, 4176–4179.
11. Fox, A.S., Oler, J.A., Shelton, S.E., Nanda, S.A., Davidson, R.J., Roseboom, P.H., and Kalin, N.H. (2012). Central amygdala nucleus (Ce) gene expression linked to increased trait-like Ce metabolism and anxious temperament in young primates. Proc. Natl. Acad. Sci. USA *109*, 18108–18113.
12. Kalin, N.H., and Shelton, S.E. (1989). Defensive behaviors in infant rhesus monkeys: environmental cues and neurochemical regulation. Science *243*, 1718–1721.
13. Nelson, E.E., and Winslow, J.T. (2009). Non-human primates: model animals for developmental psychopathology. Neuropsychopharmacology *34*, 90–105.
14. Kalin, N.H., and Shelton, S.E. (2003). Nonhuman primate models to study anxiety, emotion regulation, and psychopathology. Ann. N Y Acad. Sci. *1008*, 189–200.
15. Birn, R.M., Shackman, A.J., Oler, J.A., Williams, L.E., McFarlin, D.R., Rogers, G.M., Shelton, S.E., Alexander, A.L., Pine, D.S., Slattery, M.J., et al. (2014). Evolutionarily conserved prefrontal-amygdalar dysfunction in early-life anxiety. Mol. Psychiatry *19*, 915–922.
16. Tromp, D.P.M., Fox, A.S., Oler, J.A., Alexander, A.L., and Kalin, N.H. (2019). The Relationship Between the Uncinate Fasciculus and Anxious Temperament Is Evolutionarily Conserved and Sexually Dimorphic. Biol. Psychiatry *86*, 890–898.
17. Tromp, D.P.M., Williams, L.E., Fox, A.S., Oler, J.A., Roseboom, P.H., Rogers, G.M., Benson, B.E., Alexander, A.L., Pine, D.S., and Kalin, N.H. (2019). Altered Uncinate Fasciculus Microstructure in Childhood Anxiety Disorders in Boys But Not Girls. Am. J. Psychiatry *176*, 208–216.
18. Garbarini, N. (2010). Primates as a model for research. Dis. Model. Mech. *3*, 15–19.
19. Kalin, N.H., Shelton, S.E., and Davidson, R.J. (2004). The role of the central nucleus of the amygdala in mediating fear and anxiety in the primate. J. Neurosci. *24*, 5506–5515.
20. Armbruster, B.N., Li, X., Pausch, M.H., Herlitze, S., and Roth, B.L. (2007). Evolving the lock to fit the key to create a family of G protein-coupled receptors potently activated by an inert ligand. Proc. Natl. Acad. Sci. USA *104*, 5163–5168.
21. Sternson, S.M., and Roth, B.L. (2014). Chemogenetic tools to interrogate brain functions. Annu. Rev. Neurosci. *37*, 387–407.
22. Roth, B.L. (2016). DREADDs for Neuroscientists. Neuron *89*, 683–694.
23. Galvan, A., Raper, J., Hu, X., Paré, J.F., Bonaventura, J., Richie, C.T., Michaelides, M., Mueller, S.A.L., Roseboom, P.H., Oler, J.A., et al. (2019). Ultrastructural localization of DREADDs in monkeys. Eur. J. Neurosci. *50*, 2801–2813.
24. Fredericks, J.M., Fujimoto, A., and Rudebeck, P.H. (2019). Trust, but verify: A cautionary tale of translating chemogenetic methods (A commentray on Galvan et al). Eur. J. Neurosci. *50*, 2751–2754.
25. Eldridge, M.A., Aguilar, B.L., Baxter, M.G., Bourne, J.A., Cuzon Carlson, V.C., Deverman, B.E., et al. (2020). Workshop report: chemogenetic technology for systems neuroscience research in non-human primates 2016. OSF Preprints.
26. Eldridge, M.A., Lerchner, W., Saunders, R.C., Kaneko, H., Krausz, K.W., Gonzalez, F.J., Ji, B., Higuchi, M., Minamimoto, T., and Richmond, B.J. (2016). Chemogenetic disconnection of monkey orbitofrontal and rhinal cortex reversibly disrupts reward value. Nat. Neurosci. *19*, 37–39.
27. Grayson, D.S., Bliss-Moreau, E., Machado, C.J., Bennett, J., Shen, K., Grant, K.A., Fair, D.A., and Amaral, D.G. (2016). The Rhesus Monkey Connectome Predicts Disrupted Functional Networks Resulting from Pharmacogenetic Inactivation of the Amygdala. Neuron *91*, 453–466.
28. Nagai, Y., Kikuchi, E., Lerchner, W., Inoue, K.I., Ji, B., Eldridge, M.A., Kaneko, H., Kimura, Y., Oh-Nishi, A., Hori, Y., et al. (2016). PET imaging-guided chemogenetic silencing reveals a critical role of primate rostromedial caudate in reward evaluation. Nat. Commun. *7*, 13605.
29. Upright, N.A., Brookshire, S.W., Schnebelen, W., Damatac, C.G., Hof, P.R., Browning, P.G.F., Croxson, P.L., Rudebeck, P.H., and Baxter, M.G. (2018). Behavioral Effect of Chemogenetic Inhibition Is Directly Related to Receptor Transduction Levels in Rhesus Monkeys. J. Neurosci. *38*, 7969–7975.
30. Bonaventura, J., Eldridge, M.A.G., Hu, F., Gomez, J.L., Sanchez-Soto, M., Abramyan, A.M., Lam, S., Boehm, M.A., Ruiz, C., Farrell, M.R., et al. (2019). High-potency ligands for DREADD imaging and activation in rodents and monkeys. Nat. Commun. *10*, 4627.
31. Raper, J., Murphy, L., Richardson, R., Romm, Z., Kovacs-Balint, Z., Payne, C., and Galvan, A. (2019). Chemogenetic Inhibition of the Amygdala Modulates Emotional Behavior Expression in Infant Rhesus Monkeys. eNeuro *6*, ENEURO.0360-19.2019.
32. Upright, N.A., and Baxter, M.G. (2020). Effect of chemogenetic actuator drugs on prefrontal cortex-dependent working memory in nonhuman primates. Neuropsychopharmacology *45*, 1793–1798.
33. Hayashi, T., Akikawa, R., Kawasaki, K., Egawa, J., Minamimoto, T., Kobayashi, K., Kato, S., Hori, Y., Nagai, Y., Iijima, A., et al. (2020). Macaques Exhibit Implicit Gaze Bias Anticipating Others' False-Belief-Driven Actions via Medial Prefrontal Cortex. Cell Rep. *30*, 4433–4444.e5.
34. Nagai, Y., Miyakawa, N., Takuwa, H., Hori, Y., Oyama, K., Ji, B., Takahashi, M., Huang, X.P., Slocum, S.T., DiBerto, J.F., et al. (2020). Deschloroclozapine, a potent and selective chemogenetic actuator enables rapid neuronal and behavioral modulations in mice and monkeys. Nat. Neurosci. *23*, 1157–1167.
35. Wess, J., Nakajima, K., and Jain, S. (2013). Novel designer receptors to probe GPCR signaling and physiology. Trends Pharmacol. Sci. *34*, 385–392.
36. Gomez, J.L., Bonaventura, J., Lesniak, W., Mathews, W.B., Sysa-Shah, P., Rodriguez, L.A., Ellis, R.J., Richie, C.T., Harvey, B.K., Dannals, R.F., et al. (2017). Chemogenetics revealed: DREADD occupancy and activation via converted clozapine. Science *357*, 503–507.
37. Raper, J., Morrison, R.D., Daniels, J.S., Howell, L., Bachevalier, J., Wichmann, T., and Galvan, A. (2017). Metabolism and Distribution of Clozapine-N-oxide: Implications for Nonhuman Primate Chemogenetics. ACS Chem. Neurosci. *8*, 1570–1576.
38. Chang, W.H., Lin, S.K., Lane, H.Y., Wei, F.C., Hu, W.H., Lam, Y.W., and Jann, M.W. (1998). Reversible metabolism of clozapine and clozapine N-oxide in schizophrenic patients. Prog. Neuropsychopharmacol. Biol. Psychiatry *22*, 723–739.
39. Jann, M.W., Lam, Y.W., and Chang, W.H. (1994). Rapid formation of clozapine in guinea-pigs and man following clozapine-N-oxide administration. Arch. Int. Pharmacodyn. Ther. *328*, 243–250.
40. MacLaren, D.A., Browne, R.W., Shaw, J.K., Krishnan Radhakrishnan, S., Khare, P., España, R.A., and Clark, S.D. (2016). Clozapine N-Oxide Administration Produces Behavioral Effects in Long-Evans Rats: Implications for Designing DREADD Experiments. eNeuro *3*, ENEURO.0219-16.2016.
41. Manvich, D.F., Webster, K.A., Foster, S.L., Farrell, M.S., Ritchie, J.C., Porter, J.H., and Weinshenker, D. (2018). The DREADD agonist clozapine N-oxide (CNO) is reverse-metabolized to clozapine and produces clozapine-like interoceptive stimulus effects in rats and mice. Sci. Rep. *8*, 3840.
42. Ji, B., Kaneko, H., Minamimoto, T., Inoue, H., Takeuchi, H., Kumata, K., Zhang, M.R., Aoki, I., Seki, C., Ono, M., et al. (2016). Multimodal Imaging for DREADD-Expressing Neurons in Living Brain and Their Application to Implantation of iPSC-Derived Neural Progenitors. J. Neurosci. *36*, 11544–11558.
43. Paxinos, G., Huang, X.-F., Petrides, M., and Toga, A.W. (2009). The Rhesus Monkey Brain in Stereotaxic Coordinates (Academic Press).

44. Gunn, R.N., Lammertsma, A.A., Hume, S.P., and Cunningham, V.J. (1997). Parametric imaging of ligand-receptor binding in PET using a simplified reference region model. Neuroimage *6*, 279–287.

45. Wu, Y., and Carson, R.E. (2002). Noise reduction in the simplified reference tissue model for neuroreceptor functional imaging. J. Cereb. Blood Flow Metab. *22*, 1440–1452.

46. Wenthur, C.J., and Lindsley, C.W. (2013). Classics in chemical neuroscience: clozapine. ACS Chem. Neurosci. *4*, 1018–1025.

47. Yadav, P.N., Abbas, A.I., Farrell, M.S., Setola, V., Sciaky, N., Huang, X.P., Kroeze, W.K., Crawford, L.K., Piel, D.A., Keiser, M.J., et al. (2011). The presynaptic component of the serotonergic system is required for clozapine's efficacy. Neuropsychopharmacology *36*, 638–651.

48. Machado, C.J., and Bachevalier, J. (2008). Behavioral and hormonal reactivity to threat: effects of selective amygdala, hippocampal or orbital frontal lesions in monkeys. Psychoneuroendocrinology *33*, 926–941.

49. Davis, M. (2000). The role of the amygdala in conditioned and unconditioned fear and anxiety. In In The Amygdala: A Functional Analysis, *2nd edition*, J. Aggleton, ed (Oxford), pp. 213–287.

50. Agustín-Pavón, C., Braesicke, K., Shiba, Y., Santangelo, A.M., Mikheenko, Y., Cockroft, G., Asma, F., Clarke, H., Man, M.S., and Roberts, A.C. (2012). Lesions of ventrolateral prefrontal or anterior orbitofrontal cortex in primates heighten negative emotion. Biol. Psychiatry *72*, 266–272.

51. Su, X., Kells, A.P., Salegio, E.A., Salegio, E.A., Richardson, R.M., Hadaczek, P., Beyer, J., Bringas, J., Pivirotto, P., Forsayeth, J., and Bankiewicz, K.S. (2010). Real-time MR imaging with Gadoteridol predicts distribution of transgenes after convection-enhanced delivery of AAV2 vectors. Mol. Ther. *18*, 1490–1495.

52. Kalin, N.H., Fox, A.S., Kovner, R., Riedel, M.K., Fekete, E.M., Roseboom, P.H., Tromp, P.M., Grabow, B.P., Olsen, M.E., Brodsky, E.K., et al. (2016). Overexpressing corticotropin-releasing factor in the primate amygdala increases anxious temperament and alters its neural circuit. Biol. Psychiatry *80*, 345–355.

53. Spampanato, J., Polepalli, J., and Sah, P. (2011). Interneurons in the basolateral amygdala. Neuropharmacology *60*, 765–773.

54. McDonald, A.J. (1992). Cell types and intrinsic connections of the amygdala. In The Amygdala: Neurobiological Aspects of Emotion, Memory, and Mental Dysfunction, J.P. Aggleton, ed. (Wiley-Liss), pp. 67–96.

55. McDonald, A.J., and Augustine, J.R. (1993). Localization of GABA-like immunoreactivity in the monkey amygdala. Neuroscience *52*, 281–294.

56. Ghashghaei, H.T., and Barbas, H. (2002). Pathways for emotion: interactions of prefrontal and anterior temporal pathways in the amygdala of the rhesus monkey. Neuroscience *115*, 1261–1279.

57. Timbie, C., García-Cabezas, M.A., Zikopoulos, B., and Barbas, H. (2020). Organization of primate amygdalar-thalamic pathways for emotions. PLoS Biol. *18*, e3000639.

58. Amaral, D.G., and Price, J.L. (1984). Amygdalo-cortical projections in the monkey (Macaca fascicularis). J. Comp. Neurol. *230*, 465–496.

59. Aggleton, J.P., Wright, N.F., Rosene, D.L., and Saunders, R.C. (2015). Complementary patterns of direct amygdala and hippocampal projections to the macaque prefrontal cortex. Cereb. Cortex *25*, 4351–4373.

60. Saunders, R.C., Rosene, D.L., and Van Hoesen, G.W. (1988). Comparison of the efferents of the amygdala and the hippocampal formation in the rhesus monkey: II. Reciprocal and non-reciprocal connections. J. Comp. Neurol. *271*, 185–207.

61. Wang, J., and Barbas, H. (2018). Specificity of Primate Amygdalar Pathways to Hippocampus. J. Neurosci. *38*, 10019–10041.

62. Davis, M., and Whalen, P.J. (2001). The amygdala: vigilance and emotion. Mol. Psychiatry *6*, 13–34.

63. Duvarci, S., and Pare, D. (2014). Amygdala microcircuits controlling learned fear. Neuron *82*, 966–980.

64. Janak, P.H., and Tye, K.M. (2015). From circuits to behaviour in the amygdala. Nature *517*, 284–292.

65. McDonald, A.J. (2020). Functional neuroanatomy of the basolateral amygdala: Neurons, neurotransmitters, and circuits. In Handbook of Behavioral Neuroscience, *Volume 26*, J.H. Urban and J.A. Rosenkranz, eds. Handbook of Behavioral Neuroscience (Elsevier), pp. 1–38.

66. Ehrlich, I., Humeau, Y., Grenier, F., Ciocchi, S., Herry, C., and Lüthi, A. (2009). Amygdala inhibitory circuits and the control of fear memory. Neuron *62*, 757–771.

67. Felix-Ortiz, A.C., Beyeler, A., Seo, C., Leppla, C.A., Wildes, C.P., and Tye, K.M. (2013). BLA to vHPC inputs modulate anxiety-related behaviors. Neuron *79*, 658–664.

68. Tye, K.M., Prakash, R., Kim, S.Y., Fenno, L.E., Grosenick, L., Zarabi, H., Thompson, K.R., Gradinaru, V., Ramakrishnan, C., and Deisseroth, K. (2011). Amygdala circuitry mediating reversible and bidirectional control of anxiety. Nature *471*, 358–362.

69. Etkin, A., Prater, K.E., Schatzberg, A.F., Menon, V., and Greicius, M.D. (2009). Disrupted amygdalar subregion functional connectivity and evidence of a compensatory network in generalized anxiety disorder. Arch. Gen. Psychiatry *66*, 1361–1372.

70. Fox, A.S., Oler, J.A., Tromp, P.M., Fudge, J.L., and Kalin, N.H. (2015). Extending the amygdala in theories of threat processing. Trends Neurosci. *38*, 319–329.

71. Oler, J.A., Fox, A.S., Shackman, A.J., and Kalin, N.H. (2016). The central nucleus of the amygdala is a critical substrate for individual differences in anxiety. In Living Without an Amygdala, D.G. Amaral and R. Adolphs, eds. (Guilford Press), pp. 218–251.

72. Paré, D., Quirk, G.J., and Ledoux, J.E. (2004). New vistas on amygdala networks in conditioned fear. J. Neurophysiol. *92*, 1–9.

73. Zikopoulos, B., John, Y.J., García-Cabezas, M.A., Bunce, J.G., and Barbas, H. (2016). The intercalated nuclear complex of the primate amygdala. Neuroscience *330*, 267–290.

74. Fox, A.S., Souaiaia, T., Oler, J.A., Kovner, R., Kim, J.M.H., Nguyen, J., French, D.A., Riedel, M.K., Fekete, E.M., Rabska, M.R., et al. (2019). Dorsal amygdala neurotrophin-3 decreases anxious temperament in primates. Biol. Psychiatry *86*, 881–889.

75. Han, W., Tellez, L.A., Rangel, M.J., Jr., Motta, S.C., Zhang, X., Perez, I.O., Canteras, N.S., Shammah-Lagnado, S.J., van den Pol, A.N., and de Araujo, I.E. (2017). Integrated Control of Predatory Hunting by the Central Nucleus of the Amygdala. Cell *168*, 311–324.e18.

76. Hartley, N.D., Gaulden, A.D., Báldi, R., Winters, N.D., Salimando, G.J., Rosas-Vidal, L.E., Jameson, A., Winder, D.G., and Patel, S. (2019). Dynamic remodeling of a basolateral-to-central amygdala glutamatergic circuit across fear states. Nat. Neurosci. *22*, 2000–2012.

77. Steinberg, E.E., Gore, F., Heifets, B.D., Taylor, M.D., Norville, Z.C., Beier, K.T., Földy, C., Lerner, T.N., Luo, L., Deisseroth, K., and Malenka, R.C. (2020). Amygdala-Midbrain Connections Modulate Appetitive and Aversive Learning. Neuron *106*, 1026–1043.e9.

78. Kalin, N.H. (1993). The neurobiology of fear. Sci. Am. *268*, 94–101.

79. Emborg, M.E., Joers, V., Fisher, R., Brunner, K., Carter, V., Ross, C., Raghavan, R., Brady, M., Raschke, J., Kubota, K., and Alexander, A. (2010). Intraoperative intracerebral MRI-guided navigation for accurate targeting in nonhuman primates. Cell Transplant. *19*, 1587–1597.

80. Emborg, M.E., Hurley, S.A., Joers, V., Tromp, P.M., Swanson, C.R., Ohshima-Hosoyama, S., Bondarenko, V., Cummisford, K., Sonnemans, M., Hermening, S., et al. (2014). Titer and product affect the distribution of gene expression after intraputaminal convection-enhanced delivery. Stereotact. Funct. Neurosurg. *92*, 182–194.

81. Amaral, D.G., and Bassett, J.L. (1989). Cholinergic innervation of the monkey amygdala: an immunohistochemical analysis with antisera to choline acetyltransferase. J. Comp. Neurol. *281*, 337–361.

82. Jewett, D.M. (1992). A simple synthesis of [11C]methyl triflate. Int. J. Rad. Appl. Instrum. [A] *43*, 1383–1385.

83. Larsen, P., Ulin, J., Dahlstrom, K., and Jensen, M. (1997). Synthesis of [11C]iodomethane by iodination of [11C]methane. Appl. Radiat. Isot. *48*, 153–157.

84. Avants, B.B., Tustison, N.J., Song, G., Cook, P.A., Klein, A., and Gee, J.C. (2011). A reproducible evaluation of ANTs similarity metric performance in brain image registration. Neuroimage *54*, 2033–2044.

85. Avants, B.B., Yushkevich, P., Pluta, J., Minkoff, D., Korczykowski, M., Detre, J., and Gee, J.C. (2010). The optimal template effect in hippocampus studies of diseased populations. Neuroimage *49*, 2457–2466.